Hydrol. Earth Syst. Sci. Discuss., https://doi.org/10.5194/hess-2018-279
Manuscript under review for journal Hydrol. Earth Syst. Sci.
Discussion started: 18 July 2018

Hydrology and Earth System Sciences
Open Access
Discussions

Impact of skin effect on single-well push-pull tests with the presence of regional groundwater flow

Xu Li[a], Zhang Wen[a]*, Hongbin Zhan[a,b], Qi Zhu[a]

[a]School of Environmental Studies, China University of Geosciences, Wuhan, 430074, China

[b]Department of Geology and Geophysics, Texas A & M University, College Station, TX 77843-3115, USA, Email: zhan@geo.tamu.edu

*Corresponding author: Zhang Wen, Ph.D. Professor. Affiliation: School of Environmental Studies, China University of Geosciences, Wuhan, Hubei, 430074, P. R. China. Email: wenz@cug.edu.cn. Tel: 86-27-67883159. Fax: 86-27-87436235.

Hydrol. Earth Syst. Sci. Discuss., https://doi.org/10.5194/hess-2018-279
Manuscript under review for journal Hydrol. Earth Syst. Sci.
Discussion started: 18 July 2018

Hydrology and Earth System Sciences
Discussions

Abstract

Single-well push-pull (SWPP) test is one of the most important ways to estimate aquifer transport parameters, e.g. porosity, dispersivity, rate of biogeochemical reaction, but its application for determining the regional groundwater velocity has rarely been discussed in previous studies. In this study, a new numerical model of SWPP test considering regional groundwater flow and skin effects was established using the finite-element COMSOL Multiphysics. The effects of regional groundwater flow velocity and skin properties on breakthrough curves (BTCs) were thoroughly analyzed. Several important results were obtained. Firstly, the regional groundwater velocity affects the types of BTCs through changing the pattern and location of the dividing streamline. Secondly, a positive (or negative) skin leads to a slower (or faster) tracer transport process. That is, a positive skin results in a higher concentration at early stage at a given time. Thirdly, a smaller hydraulic conductivity ratio δ of the positive skin to the formation results in greater solute plume retardation in the skin zone. Besides, a larger thickness of the positive skin leads to a higher tracer concentration around the well. The opposite is true if the skin is negative. The general conclusion is that the skin effects on SWPP test are significant and should be considered.

Keywords: push-pull test, regional groundwater velocity, solute transport, skin effect

Hydrol. Earth Syst. Sci. Discuss., https://doi.org/10.5194/hess-2018-279
Manuscript under review for journal Hydrol. Earth Syst. Sci.
Discussion started: 18 July 2018

1. Introduction

The single-well push-pull (SWPP) tests have been commonly employed to estimate aquifer parameters, e.g. regional groundwater flow velocity, porosity, dispersivity, biogeochemical reaction rate (Gelhar and Collins, 1971; Hall et al., 1991; Schroth and Istok, 2006). The process of this test can be summarized as follows: A tracer is injected into a target aquifer (push), then the mixed solution is pumped out from the same location (pull). Groundwater samples are taken at regular time intervals at the test well during the pumping process, and parameters can be obtained by fitting the observed breakthrough curves (BTCs) using a proper mathematical model. Generally, a complete SWPP test may consist of four phases: tracer injection, chasing, rest, and pumping. The chasing phase is to push the tracer away from the injection well (Istok et al., 1997), and the rest phase is for tracer to diffuse and/or react with the aquifer (if a reactive tracer is employed). Conservative or reactive tracers can be utilized, depending on the purpose of the test. In general, conservative tracers have been widely used to estimate regional groundwater flow velocity, porosity, and dispersivity, etc. (Leap and Kaplan, 1988; Haggerty et al., 2001; Hebig-Schubert, 2014). Similarly, one can obtain the information of sorption, cation exchange, microbial processes by applying reactive tracers (Trudell et al., 1986; Field et al., 2000; Tong et al., 2016). For instance, Tong et al. (2016) used SWPP tests to validate the abundant production of hydroxyl radicals due to the oxidization of subsurface sediments.

To interpret the SWPP test results, a proper mathematical model considering the fundamental physical and biogeochemical processes of the test is indispensable (Haggerty et al., 2001; Kleikemper et al., 2002; Schroth and Istok, 2006). From a transport perspective,

many existing models are governed by the conventional advection-dispersion equation (ADE), assuming the validity of Fick's law in the SWPP tests (Schroth et al., 2000; Huang et al., 2010). Subsequently, many analytical and numerical solutions of various single-well models have been developed. For instance, Huang et al. (2010) obtained an exact analytical solution of SWPP test by using Fick's law, considering a partially penetrating well in the aquifer. Besides ADE, a number of non-Fickian transport models of SWPP tests have also been developed in recent years to recognize the influence of media heterogeneity, especially in fractured aquifers (Chen et al., 2017). Such models include multi-rate mass transfer models (Haggerty et al., 2001), continuous time random walk (CTRW) (Le Borgne and Gouze, 2008), and fractional advection-dispersion equation (FADE) models (Benson et al., 2004; Chen et al., 2017), to name a few. For instance, Chen et al. (2017) developed a fractional model of multistage SWPP test to simulate non-Fickian behavior for a fractured aquifer. In addition, Schroth et al. (2005) obtained an approximate analytical solution of SWPP test for spherical-flow conditions. Wang et al. (2017) investigated the impacts of transient flow and wellbore storage on SWPP test under transient Forchheimer flow using a finite-difference method.

As mentioned above, SWPP test is a powerful tool for aquifer characterization, including the determination of regional groundwater flow velocity. Traditionally, regional groundwater flow velocity can be obtained by three or more groundwater monitoring wells in the aquifer by conducting the natural gradient tracer tests rather than the SWPP tests (Pickens et al., 1981; Michie, 1996; Zimmermann and Huenges, 1999). However, the natural gradient tracer tests usually take much longer time to complete. This is particularly troublesome when the

medium is less permeable, and the regional groundwater flow velocity is relatively small (Schubert et al., 2011). The natural gradient tracer test method is also very costly to implement in deep aquifers as the installation of multiple wells in deep aquifers can be formidably expensive. In contrast, the SWPP test only needs a single well, thus can substantially reduce the cost of test, and becomes a nice alternative for the determination of regional groundwater flow velocity (Leap and Kaplan, 1988; Butler et al., 2009). To serve such a purpose, the SWPP tests usually consist of three phases: tracer injection, rest, and pumping. The rest phase allows the injected tracer to drift with regional groundwater velocity, thus it is a key phase to include. Leap and Kaplan (1988) obtained an equation for push-pull test to determine regional groundwater flow velocity in a confined aquifer, and a series of laboratory tests were conducted to verify the accuracy of the model, but the test results showed that if the solute transport drifted over the location of dividing streamline toward downstream, the calculated results of the regional flow velocity would produce a large error with the comparison to the actual value. After that, Hall et al. (1991) presented another type of SWPP test for determining regional groundwater velocity and effective porosity based on the method of Leap and Kaplan (1988), but Hall et al. (1991) required a directly downgradient monitoring well. It is notable that both approaches mentioned above have some limitations for determining regional groundwater velocity.

In addition, the impacts of skin near a pumping well are usually neglected for a SWPP test, which might bring about great errors for the estimation of aquifer parameters and regional groundwater flow velocity. During the process of well implementation, the intrusion of drilling mud into the aquifer in the vicinity of well is inevitable, which can result in the

change of the porosity and permeability surrounding the well screen (Hurst et al., 1969). This phenomenon can be regarded as the skin effect (Chen and Chang, 2002; Wang et al., 2012). The thickness of skin usually ranges from a few millimeters to several meters (Novakowski, 1989). The skins can be classified into positive and negative types according to the hydraulic conductivity contrast between the skin and the formation zone. If the hydraulic conductivity of the skin is smaller than that of the formation zone, the skin is defined as a positive one. Otherwise, it is a negative skin (Park and Zhan, 2002; Yeh et al., 2003; Wen et al., 2011). Such a skin, regardless of positive or negative, will inevitably alter the flow field near the test well, thus its effect must be taken into consideration for interpreting the SWPP test. For instance, the streamlines of skin zone can converge toward the well in the case of a negative skin, but the opposite is true for a positive skin (Drost et al., 1968; Schubert et al., 2011).

In summary, the skin effect is a very important issue from the perspective of SWPP test interpretation. Through a careful check on the literature, we notice that the model of SWPP for estimating groundwater flow velocity needs further investigation, besides, the impacts of skin effects on SWPP tests for estimating groundwater flow velocity have rarely been studied, which will be the purpose of this study. To accomplish the objective, we will investigate a SWPP test containing three phases of injection, rest and pumping using a fully penetrating well. We will use the finite-element COMSOL Multiphysics to numerically simulate the steady-state, two-dimensional (2D) horizontal flow, with specific attention paid to the skin effect.

2. Mathematical model of the SWPP test

Hydrol. Earth Syst. Sci. Discuss., https://doi.org/10.5194/hess-2018-279
Manuscript under review for journal Hydrol. Earth Syst. Sci.
Discussion started: 18 July 2018

To illustrate the problem, we will use a conservative tracer. A confined aquifer is assumed to be unbounded laterally with a uniform regional groundwater flow presented over the entire duration of test. The aquifer is assumed to be homogeneous and horizontally isotropic. A fully penetrating well is used so only the horizontal flow is of concern here. Flow is assumed to be Darcian and transport is assumed to be Fickian. The test well radius is assumed to be sufficiently small so that the wellbore effect is not a concern. The tracer is injected with a constant rate and a constant concentration at the injection phase and is pumped with a constant rate (which could be different from the injection rate) at the pumping phase, after a certain period of rest phase to allow the injected tracer drifting with the regional groundwater flow. The coordinate system is established as follows with the origin at the center of the test well and the *x*-axis pointing to the direction of regional groundwater flow. A 2D schematic diagram investigated here is depicted in Fig.1.

2.1 Mathematical model of groundwater flow

Flow of the SWPP test is assumed to be steady-state, thus the groundwater flow velocity can be expressed as the superposition of the flow component generated by the pumping well and the regional flow:

$$\vec{v} = \vec{v}_1 + \vec{v}_2 \quad (1)$$

$$\vec{v}_1 = v_1\vec{e}_r = Q/\left(2\pi\theta Br\right)\vec{e}_r \quad (2)$$

$$\vec{v}_2 = v_2\vec{e}_x = \left(-KJ/\theta\right)\vec{e}_x = \left(v_d/\theta\right)\vec{e}_x \quad (3)$$

$$r = \sqrt{x^2 + y^2} \quad (4)$$

where the arrow over a symbol represents a vector hereinafter; $\vec{v}_1$ is the average radial pore velocity vector generated by the injection (or pumping well) with a magnitude of v_1 [L/T]and

Hydrol. Earth Syst. Sci. Discuss., https://doi.org/10.5194/hess-2018-279
Manuscript under review for journal Hydrol. Earth Syst. Sci.
Discussion started: 18 July 2018

144 $\vec{e}_r$ is a unit vector along the radial direction; $\vec{v}_2$ is the regional groundwater pore flow
145 velocity vector with a magnitude of v_2 [L/T] and v_d is the regional groundwater Darcy flow
146 velocity, and $\vec{e}_x$ is a unit vector long the *x*-axis; $\vec{v}$ is the lumped groundwater flow velocity
147 near the well [L/T]; *B* is the aquifer thickness [L]; *r* is the radial distance [L]; *Q* is the
148 injection or pumping rate [L^3/T], which is positive for the injection and negative for pumping,
149 and *Q* is 0 during the rest phase; *K* is aquifer hydraulic conductivity [L/T]; *J* is the hydraulic
150 gradient of regional flow [L/L]; θ is the aquifer effective porosity [dimensionless], which is
151 assumed to be the same as the total porosity of the aquifer when all the pore spaces are well-
152 connected with negligible immobile porosity; *r* is the radial distance [L] from the well and *x*
153 and *y* are two horizontal coordinates [L], parallel and perpendicular to the regional
154 groundwater flow direction, respectively.

155 According to Fig.1, the boundary conditions for the domain of concern can be expressed
156 as:

157 $$H(x,y)\big|_{s_1} = H_1, \quad H(x,y)\big|_{s_2} = H_2 \tag{5}$$

158 $$K\frac{\partial H}{\partial n}\bigg|_{s_3} = 0, \quad K\frac{\partial H}{\partial n}\bigg|_{s_4} = 0 \tag{6}$$

159 where s_1, s_2 ,s_3 and s_4 are the boundaries of the model; s_1 and s_2 are constant-head boundaries
160 with prescribed heads of $H_1$and H_2, respectively; both s_3 and s_4 are no-flux boundaries.
161 Therefore, a constant regional flow field can be generated and one can obtain different values
162 of v_2 by changing the head differences of H_1 and H_2.

163 **2.2 Mathematical model of solute transport**

164 The ADE of a conservative solute without source/sink can be written as:

Hydrol. Earth Syst. Sci. Discuss., https://doi.org/10.5194/hess-2018-279
Manuscript under review for journal Hydrol. Earth Syst. Sci.
Discussion started: 18 July 2018

Hydrology and Earth System Sciences
Discussions

$$\frac{\partial C}{\partial t} = \nabla \cdot \left(D \nabla C \right) - \nabla \cdot \left(\vec{v} C \right) \quad (7)$$

where C is the solute concentration [M/L^3]; t is the transport time [T]; D is the hydrodynamic dispersion [L^2/T]; $\nabla \cdot$ and ∇ are the divergence operator and the gradient operator respectively; the hydrodynamic dispersion is a velocity-dependent tensor depicted as:

$$D_{xx} = \frac{\alpha_L v_x^2}{\left| \vec{v} \right|} + \frac{\alpha_T v_y^2}{\left| \vec{v} \right|} + D_{diff} \quad (8)$$

$$D_{yy} = \frac{\alpha_L v_y^2}{\left| \vec{v} \right|} + \frac{\alpha_T v_x^2}{\left| \vec{v} \right|} + D_{diff} \quad (9)$$

$$D_{xy} = D_{yx} = \left(\alpha_L - \alpha_T \right) \frac{v_x v_y}{\left| \vec{v} \right|} \quad (10)$$

$$v = \sqrt{v_x^2 + v_y^2} \quad (11)$$

where D_{xx}, D_{xy}, and D_{yy} are components of the hydrodynamic dispersion coefficient tensor [L^2/T]; D_{diff} is the molecular diffusion coefficient [L^2/T]; α_L is the longitudinal dispersivity [L]; α_T is the transverse dispersivity [L]; the transverse dispersion effect is much smaller, thus one usually assumes $\alpha_L = 10\alpha_T$ (Guvanasen and Guvanasen, 1987; Chen et al., 1999; Chen et al., 2006); v_x is pore velocity in the x direction; v_y is pore velocity in the y direction.

The initial condition is:

$$C\left(r,0\right) = 0\,, \quad (12)$$

During the injection phase, the inner boundary condition inside the well can be described as:

$$C\left(r,t\right) = C_0, \qquad r = r_w, 0 < t < t_{inj} \quad (13)$$

where C_0 represents the concentration of the injection phase [M/L^3]; r_w is the well radius [L]; t_{inj} is the duration of the injection phase [T]. The third-type boundary condition may also be

Hydrol. Earth Syst. Sci. Discuss., https://doi.org/10.5194/hess-2018-279
Manuscript under review for journal Hydrol. Earth Syst. Sci.
Discussion started: 18 July 2018

used to replace the first-type boundary condition of Eq. (13). However, our numerical exercises indicate that both conditions yield nearly the same results except for a very short period of time since the start of injection. Therefore, without loss of generality, we use the first-type boundary condition here as an example to illustrate the methodology.

During the rest phase, the solute flux from the borehole into the aquifer is zero, but the solute concentration around the borehole is nonzero, therefore, rather than a constant concentration boundary, a constant-flux (or the third-type) boundary is more reasonable and can be described as:

$$v_1 C - D\frac{\partial C}{\partial r}\Big|_{r\to r_w^-} = 0, \qquad t_{inj} < t < t_{res} \tag{14}$$

where t_{res} is the duration of the rest phase [T]. Eq. (14) represents a zero-flux boundary. During the rest phase, Q is 0.

During the pumping phase, the time-dependent concentration is measured in the borehole. The main target of the test is to obtain several parameters by fitting the observed breakthrough curves (BTCs) with corresponding theoretical BTCs obtained from a proper analytical or numerical solution. When solute transport through well screen, the boundary condition at the well screen is (Wang et al., 2017):

$$\frac{\partial C}{\partial r}\Big|_{r\to r_w^-} = 0 \tag{15}$$

Because the values of velocity and concentration are different around the perimeter of the borehole, it is necessary to integrate the concentration around the borehole with the velocity as the weight to obtain the accurate value of concentration at the well, thus, the flux-averaged concentrations can be expressed as:

Hydrol. Earth Syst. Sci. Discuss., https://doi.org/10.5194/hess-2018-279
Manuscript under review for journal Hydrol. Earth Syst. Sci.
Discussion started: 18 July 2018

$$\overline{C} = \frac{\oint_{l_w} v_w C_w}{\oint_{l_w} v_w}, \qquad r = r_w, t_{res} < t < t_{pump} \tag{16}$$

where v_w represents the superposition velocity around the borehole during the pumping [L/T]; C_w represents the concentration around the well perimeter [M/L3]; $\overline{C}$ is the concentration inside the well [M/L3]; l_w is the perimeter of the wellbore [L].

3. Numerical solution of the SWPP test

In this study, a steady-state flow model of 2D horizontal plane was developed based on COMSOL Multiphysics, as shown in Fig. 1. The model region was set to be 40 m×40 m, and the well has a radius of 0.1 m. In addition, B=10 m, K=8.0 m/d, θ=0.3. In this model, constant-head boundaries were prescribed, and the value of H_2 was set as constant 15 m, according to Eq. (3), one can obtain different values of v_2 by changing the value of H_1. In the model, a continuous mass flux of injection or pumping rate was assigned at r=r_w, which can be expressed as:

$$N_0 = \frac{Q\rho}{2\pi r_w B} \tag{17}$$

where, N_0 is the mass flux per unit thickness [M/L^2/T]; ρ is the density of groundwater [M/L^3]. The SWPP test was divided into three phases, the simulation results at the end of each phase, including the hydraulic head and the solute concentration, were set as the initial values for the simulation in the next phase.

A uniform skin near the well was considered in a confined aquifer, and the thickness of the well skin was assumed to be constant and equal to r_s along the well screen in this model. The skin hydraulic conductivity and effective porosity were set as K_s and θ_s respectively. The default values of the parameters were shown in Table 1.

Hydrol. Earth Syst. Sci. Discuss., https://doi.org/10.5194/hess-2018-279
Manuscript under review for journal Hydrol. Earth Syst. Sci.
Discussion started: 18 July 2018

Hydrology and Earth System Sciences
Discussions

The model domain was discretized into 21688 elements, and the mesh size was progressively refined near the well. When the number of element is doubled, the peak solute concentration for the pumping phase varied about 0.17%. Therefore the selected mesh is regarded as sufficiently fine for the problem investigated here. To check the accuracy of the numerical model further, the numerical solution for a special case (without skin) was used to compare with the analytical solution of Huang et al. (2010), who investigated a steady-state flow SWPP model with injection and extraction phases, without the regional groundwater flow, as shown in Fig.2. The simulated time span of tracer injection and pumping were 0.5 and 1 day, respectively. The other parameters were given as: Q_{inj}= 50 m^3/d, Q_{pump}=-50 m^3/d, B=10 m, α_L=0.1 m, 0.5 m, 1 m, and θ=0.3. C_0 at $r=r_w$ was set as 1.0 mol/m^3. The results showed that our numerical solution agreed perfectly with the analytical solution. For the following analysis, the default values of the parameters are listed in Table 1.

4. Results and discussions

4.1. Effects of regional groundwater velocity on BTCs in the SWPP test

Fig. 3 shows the BTCs for the pumping phase with different regional groundwater velocities, like 5×10^{-7} m/s, 1×10^{-6} m/s, 1.5×10^{-6}m/s, 2×10^{-6} m/s, 2.5×10^{-6} and 3×10^{-6} m/s. Besides, α_L =0.1 m, Q_{inj}= 30 m^3/d, Q_{pump}=-15 m^3/d, and the other parameters are the same as those used in Table 1. It is found that different regional groundwater velocities have great impacts on BTCs, and such impacts depend on the value of the regional groundwater velocities. It is found that the tracer concentration is smaller at early stage with a greater regional groundwater velocity. Additionally, it is notable that a larger regional groundwater velocity will result in a longer tailing.

Hydrol. Earth Syst. Sci. Discuss., https://doi.org/10.5194/hess-2018-279
Manuscript under review for journal Hydrol. Earth Syst. Sci.
Discussion started: 18 July 2018

Fig. 4 shows the superposition of flow components generated by the pumping well and the regional flow. For the pumping phase, one can see that there is a stagnation point (Sp) located at the dividing streamline (Ds) as shown in Fig.4. For a single tracer particle, whether it can be extracted out from the aquifer depends on the pattern and location of the dividing line, which acts like a fishing net to collect all the products together. Therefore, different convergence situations of tracer due to variable dividing streamlines result in a series of BTC types. In order to interpret this behavior explicitly, the concentration distributions in a 2D horizontal plane at t_{pump}=0 hr with different regional groundwater velocities are shown in Fig. 5. One can see that a certain amount of tracer mass may be retained near the symmetry axis (x-axis) and around the well when the regional groundwater velocity is relatively low, such as v_d=1×10^{-6} m/s and 1.5×10^{-6} m/s, as shown in Figs.5a-5b, resulting in relatively high concentrations in the wellbore at early stage. On the contrary, a larger regional groundwater velocity leads to a faster tracer transport process, causing the tracer mass drifting away from the well, as shown in Figs.5c-5d. Besides, one can also see that a larger regional groundwater velocity leads to a smaller distance from Sp to well, resulting in a smaller portion of tracer mass that can be extracted during the pumping phase. The opposite is true for the case of a smaller regional groundwater velocity. For instance, as for the tracer mass on the left side of the dividing streamline, they can be extracted by smaller velocities such as v_d=5×10^{-7} m/s and 1×10^{-6} m/s, as shown in Figs.5a-5b, but very limited tracer can be captured with larger velocities like v_d=3×10^{-6} m/s. And this further confirms the reasonability of the BTC types in Fig. 3.

4.2 The effects of t_{res} on BTCs in the SWPP test

Hydrol. Earth Syst. Sci. Discuss., https://doi.org/10.5194/hess-2018-279
Manuscript under review for journal Hydrol. Earth Syst. Sci.
Discussion started: 18 July 2018

Fig. 6 shows BTCs for the pumping phase with different t_{res}, like 6, 12, 24, and 36 hr. Besides, α_L =0.1 m, v_d =3×10^{-6} m/s, Q_{inj}=30 m^3/d, Q_{pump}=-15 m^3/d and the other parameters are the same as those used in Table 1. It is found that the tracer concentration is smaller as t_{res} increases in Fig. 6. This is because a longer time of rest phase means a farther distance of tracer drifting, leading to a smaller portion of tracer mass that can be extracted during the pumping phase. In order to interpret this behavior explicitly, the concentration distributions in a 2D horizontal plane at t_{pump}=0 hr with different t_{res} are shown in Fig. 7. One can see that a longer t_{res} means that more tracer mass drifting over the location of Sp toward downstream, resulting in lower concentrations in the wellbore during the pumping phase in Fig. 7. According to the analysis above, there is a strong interaction between regional groundwater flow and well flow, thus proper choices of the duration of each phase, and the injection and pumping rates are vital for the success of a SWPP test. For instance, for the case of a relatively large regional groundwater velocity, one can decrease t_{res} or increase the magnitude of Q_{pump} to recollect the tracer as much as possible, thus avoiding the over- or under-estimation of hydraulic parameters from the SWPP test.

4.3. The effects of porosity on BTCs in the SWPP test

Fig. 8 shows the effects of porosity θ on BTCs during the pumping phase. The parameters are given as: θ= 0.1, 0.2, 0.3, 0.4 and 0.5 respectively, v_d=3×10^{-6} m/s, α_L=0.1m, Q_{inj}=30 m^3/d, and Q_{pump}=-30 m^3/d. It can be found that the concentration is smaller at early stage with a smaller porosity. It is also obvious that a smaller θ will result in a longer tailing at late stage. The explanation is similar to that for Fig. 3, i.e., a smaller θ means a faster pore velocity, resulting in faster solute transport according to Eq. (3).

Hydrol. Earth Syst. Sci. Discuss., https://doi.org/10.5194/hess-2018-279
Manuscript under review for journal Hydrol. Earth Syst. Sci.
Discussion started: 18 July 2018

293 **4.4. The effects of dispersivity on BTCs in the SWPP test**

294 Fig. 9 shows the effect of α_L on BTCs for the pumping phase. The values of α_L are set as:
295 α_L =0.01 m, 0.05 m, 0.1 m, 0.5 m and the other parameters are given as: v_d=2×10^{-6} m/s,
296 Q_{inj}=30 m^3/d, and Q_{pump}=-30 m^3/d. As shown in Fig. 9, one can see that α_L has a significant
297 impact on BTCs. At early stage of pumping, the concentration shows a decreasing trend with
298 increase of α_L , This is because a larger dispersivity means a faster tracer transport , given the
299 same regional groundwater velocity, which causes much broader solute plume after the
300 injection and rest phases. A smaller dispersivity means a narrower solute plume. Therefore,
301 different dispersivities can change the characteristics of BTCs under the influence of regional
302 groundwater velocity.

303 **4.5. The effects of skin hydraulic conductivity on BTCs in the SWPP test**

304 As mentioned above, the well skin includes two general types, i.e., a positive skin or a
305 negative skin. Denoting the hydraulic conductivities of skin and aquifer (or formation zone)
306 respectively as K_s and K, one can use a new parameter $\delta=K_s/K$ to reflect the skin impact,
307 where δ is a parameter reflecting the type of the skin and called the "skin index" hereinafter.
308 Specifically, δ<1 represents a positive skin, while δ >1 represents a negative skin. Note that
309 the case of δ =1 represents the case without a skin. In this section, we will provide a detailed
310 analysis on the impact of the skin hydraulic conductivity on SWPP test.

311 **4.5.1 Positive skin**

312 Fig. 10 shows the effect of different skin indexes on BTCs for a positive skin case
313 during the pumping phase. The parameters are given as: v_d=3×10^{-6} m/s, Q_{inj}=30 m^3/d,
314 Q_{pump}=-30 m^3/d, α_L=0.1 m, r_s=0.6 m, δ= 1, 0.5, 0.25 and 0.125, respectively. The results

315 indicate that the concentration gets higher at early stage of pumping when the skin index is
316 lower, as shown in Fig. 10. This may be explained as follows. A skin with a lower δ value (or
317 a lower permeability value in respect to that of the formation) essentially serves as a
318 somewhat "shield" around the test well that can make the spreading of the tracer mass out of
319 the test well more difficult during the injection phase. Consequently, more tracer mass will be
320 retained near the test well either in the skin or near the skin in the formation zone. Therefore,
321 during the pumping phase of the test, more tracer mass can be extracted during the early stage
322 of the pumping phase, leading to higher concentration during that stage. To further explicitly
323 interpret this behavior, the concentration distributions in a 2D horizontal plane at t_{pump}=0 hr
324 with different δ values are shown in Fig. 11. As can be seen in Fig.11, a lower skin hydraulic
325 conductivity leads to more tracer accumulation in the skin zone after the rest phase. For
326 instance, one can see that the solute plumes with high concentrations are clearly visible in
327 skin zones for the cases of δ=0.25 and 0.125.

328 **4.5.2 Negative skin**

329 Fig. 12 shows the effect of different skin indexes on the BTCs for a negative skin case.
330 The parameters are given as: v_d=3×10^{-6} m/s, Q_{inj}= 30 m^3/d, Q_{ext}=-30 m^3/d, α_L=0.1 m, r_s=0.6
331 m, and δ=1, 1.5, 2 and 3 . In contract to what has been observed in Fig. 10 for a positive skin,
332 the results indicate that the concentration gets lower at early stage of pumping when the skin
333 index (δ) increases. This is because a negative skin is somewhat like a "high conductance
334 zone" rather than a "shield", and can facilitate the spreading of tracer mass away from the test
335 well during the injection phase. Therefore, less tracer mass will be retained near the test well
336 for a higher skin index, thus less concentration will be seen during the early stage of pumping

in the wellbore. Similar to what has been done for a positive skin in Fig. 11, the concentration distributions in a 2D horizontal plane at t_{pump}=0 hr with different skin indexes are shown in Fig. 13. It is quite obvious to see that a larger skin hydraulic conductivity leads to a less tracer concentration in the skin zone at the early stage of the pumping phase. For instance, one can see that tracer accumulation in the skin zone for the cases of δ=2 and 3 are clearly less than the cases of δ=1 and 1.5.

4.6. Effects of skin thickness on BTCs in the SWPP test

In this section, we will analyze the impacts of the skin thickness on BTCs.

4.6.1 Positive skin

Firstly, we will analyze the impacts of the skin thickness on BTCs for a positive skin case. The parameters are given as: v_d=3×10^{-6} m/s, Q_{inj}= 30 m^3/d, Q_{ext}=-30 m^3/d, δ= 0.5 (positive skin), α_L=0.1 m, and r_s= 0, 0.2, 0.4 and 0.6 m, respectively. Fig. 14 shows the effects of the skin thickness (positive skin) on BTCs during the pumping phase. One can see that the concentration gets higher at early stage with the increase of r_s. The explanation is similar to that for Fig. 10, as a thicker positive skin means a thicker "shield" surrounding the test well, preventing the injected tracer mass from spreading further away from the test well, thus leading to higher concentrations during the early stage of the extraction phase. The concentration distributions in a 2D horizontal plane at t_{pump}=0 hr with different positive skin thickness are shown in Fig. 15. It is evident that the tracer mass still accumulates in the skin zone 24 hr after the cease of the injection phase (rest phase), and the concentration is higher in the skin zone than that in the formation zone (see the case of r_s=0.6 m). Besides, more

tracer can be found in the skin region with the increase of r_s, resulting in different shapes of BTCs in Fig.14.

4.6.2 Negative skin

Similarly, we have also analyzed the impacts of the skin thickness on BTCs for a negative skin case. The parameters are given as: v_2=3×10^{-6} m/s, Q_{inj}= 30 m^3/d, Q_{ext}=-30 m^3/d, δ= 2 (negative skin), α_L=0.1 m, r_s=0, 0.2, 0.4 and 0.6m. Fig. 16 shows the effect of the skin thickness (negative skin) on BTCs during the pumping phase. At early stage, it can be found that the concentration shows a decreasing trend with the increase of r_s, and the peak values of BTCs also decrease with the increase of r_s. The explanation is similar to that for Fig. 12 as a thicker negative skin means a thicker high conductance zone surrounding the test well, which will facilitate the spreading of injected tracer mass further away from the test well. This is further supported by the concentration distributions in a 2D horizontal plane 24 hr after the cease of injection (rest phase) with different negative skin thickness, as shown in Fig.17. It is evident from Fig. 17 that a greater portion of tracer mass migrates away from the test well after the cease of injection with a greater r_s. For instance, at early stage of extraction, one can see that the BTC values in the case of r_s =0.6 m are lower than those in the case of r_s=0.2 m in Fig.16, and the tracer is transported further away from the test well in the case of r_s =0.6 m than that in the case of r_s=0.2 m in Fig.17.

5. Conclusions

In this study, a numerical model for a SWPP test with the presence of a regional groundwater flow field, considering both the positive and negative skin effects was investigated. There is a strong interaction between regional groundwater flow and well flow,

thus proper choices of the duration of each phase, and the injection and pumping rates should be done in advance before the SWPP test to recollect the tracer as much as possible. Besides, the numerical model of SWPP test can be used to obtain unknown parameters: i.e., regional groundwater velocity, effective porosity, dispersivity, and biogeochemical reaction rates, by fitting to the observed BTCs. The effects of both the hydraulic conductivities and thickness of the skin zone on BTCs had also been considered. The following conclusions can be drawn:

1. Regional groundwater velocity has a significant effect on the shape of BTCs, a lower regional groundwater velocity means that more tracer can be accumulated near the symmetry plane around the well. The opposite is true for a case of a larger regional flow velocity, resulting in a longer tailing of BTCs obtained during the extraction phase. In addition, the pattern and location of the dividing streamline determine the quantity of tracer mass extracted during the pumping phase.
2. We have proposed a skin index which is essentially the skin/formation hydraulic conductivity ratio to quantify the skin impact. A lager skin index results in a lower concentration for BTCs at early stage of pumping. On the contrary, a smaller skin index means a higher concentration for BTCs at early stage of pumping. In addition, a smaller skin index means that solute plume can accumulate more in the skin zone, otherwise, a larger skin index results in a solute plume drifting further away from the skin zone after the cease of the injection phase.
3. The impact of skin effect near a pumping well should not be neglected for SWPP test, particularly when the regional groundwater flow is presented. The positive (or negative) skin results in a faster (or lower) tracer transport process. A lager thickness of the positive

skin leads to a larger concentration of tracer near the symmetry plane around the well, but the opposite is true for the case with a negative skin.

Acknowledgements

This research was partially supported by the National Natural Science Foundation of China (Grant Numbers: 41772259, 41372253, 41521001), the Natural Science Foundation of Hubei Province, China (2018CFA085，2018CFA028), the Fundamental Research Funds for the Central Universities, China University of Geosciences (Wuhan).

References

Benson, D. A., Tadjeran, C., Meerschaert, M. M., Farnham, I., and Pohll, G.: Radial fractional-order dispersion through fractured rock, Water Resour. Res., 40(12), 87-87, 2004.

Butler, A.P., Mathias, S.A., Gallagher, A.J., Peach, D.W., and Williams, A.T.: Analysis of flow processes in fractured chalk under pumped and ambient conditions (UK), Hydrogeol J., 17(8), 1849-1858, 2009.

Chen, C. S., and Chang, C. C.: Use of cumulative volume of constant-head injection test to estimate aquifer parameters with skin effects: Field experiment and data analysis, Water Resour. Res., 38(5), 189-195, 2002.

Chen, J. S., Chen, C. S., Gau, H. S., and Liu, C. W.: A two-well method to evaluate transverse dispersivity for tracer tests in a radially convergent flow field, J. Hydrol., 223(3-4), 175-197, 1999.

Chen, K.W., Zhan, H.B., and Yang, Q: Fractional models simulating non-fickian behavior in four-stage single-well push-pull tests, Water Resour. Res., 53(11), 9528-9545, 2017.

Drost, W., Klotz, D., Koch, A., Moser, H., Neumaier, F., and Rauert, W: Point dilution methods of investigating ground water flow by means of radioisotopes, Water Resour. Res., 4(1), 125-146, 1968.

Field, J. A., Sawyer, T. E., Schroth, M. H., Humphrey, M. D., and Istok, J. D.: Effect of cation exchange on surfactant-enhanced solubilization of trichloroethene, J. Contam. Hydrol., 46(1-2), 131-149, 2000.

Gelhar, L. W., and Collins, M. A.: General analysis of longitudinal dispersion in nonuniform flow. Water Resour. Res., 7(6), 1511-1521, 1971.

Guvanasen V., and Guvanasen V M.: An approximate semianalytical solution for tracer injection tests in a confined aquifer with a radially converging flow field and finite volume of tracer and chase fluid, Water Resour. Res., 23(8), 1607-1619, 1987.

Haggerty, R., Fleming, S. W., Meigs, L. C., and McKenna, S.A.: Tracer tests in a fractured dolomite: 2. Analysis of mass transfer in single-well injection-withdrawal tests, Water Resour. Res., 37(5), 1129-1142, 2001.

Hall, S.H., Luttrell, S.P., and Cronin, W.E.: A method for estimating effective porosity and ground-water velocity, Ground Water., 29(2), 171-174, 1991.

Hebig-Schubert, K.: Deep groundwater flow systems and their characterization in single-well settings by "push-pull" tracer tests, Int. J. Fatigue., 15(5), 441, 2014.

Huang, J. Q., Christ, J. A., and Goltz, M. N.: Analytical solutions for efficient interpretation of single-well push-pull tracer tests, Water Resour. Res., 46(8), 863-863, 2010.

Hurst, W., Clark, J. D., and Brauer, E. B.: Skin effect in producing wells, J. Petrol. Technol., 21(11), 1483-1489, 1969.

Istok, J. D., Humphrey, M. D., Schroth, M. H., Hyman, M. R., and O'Reilly, K. T.: Single-well “push-pull” test for in situ determination of microbial activities, Ground Water., 35(4), 619-631, 1997.

Kleikemper, J., Pelz, O., Schroth, M. H., and Zeyer, J.: Sulfate-reducing bacterial community response to carbon source amendments in contaminated aquifer microcosms, Fems Microbiol Ecol., 42(1), 109-118, 2002.

453 Leap, D. I., Kaplan, P. G.: A single-well tracing method for estimating regional advective
454 velocity in a confined aquifer: Theory and preliminary laboratory verification. Water
455 Resour. Res., 24(7), 993-998, 1988.
456 Le Borgne, T., and Gouze, P.: Non-Fickian dispersion in porous media: 2. Model validation
457 from measurements at different scales, Water Resour. Res., 44(6), 2389-2393, 2008.
458 Michie, U.: The geological framework of the sellafield area and its relationship to
459 hydrogeology, Q. J. Eng. Geol., Hydroge. 29(Supplement_1), S13-S27, 1996.
460 Novakowski, K. S.: A composite analytical model for analysis of pumping tests affected by
461 well bore storage and finite thickness skin, Water Resour. Res., 25(9), 1937-1946, 1989.
462 Park, E. and Zhan, H. B.: Hydraulics of a finite-diameter horizontal well with wellbore
463 storage and skin effect, Adv. Water Resour., 25(4), 389-400, 2002.
464 Pickens, J. F., Jackson, R. E., Inch, K. J., and Merritt, W. F.: Measurement of distribution
465 coefficients using a radial injection dual-tracer test, Water Resour. Res., 17(3), 529-544,
466 1981.
467 Schroth, M. H., Istok, J. D., and Haggerty, R.: In situ evaluation of solute retardation using
468 ingle-well push-pull tests, Adv. Water Resour., 24(1), 105-117, 2000
469 Schroth, M. H. and Istok, J. D.: Models to determine first-order rate coefficients from single-
470 well push-pull tests, Ground Water., 44(2), 275-283, 2006.
471 Schroth, M. H., and Istok, J. D.: Approximate solution for solute transport during spherical-
472 flow push-pull tests, Ground Water., 43(2), 280-284, 2005.

473 Schubert, M., Brueggemann, L., Knoeller, K., and Schirmer, M.: Using radon as an
474 environmental tracer for estimating groundwater flow velocities in single-well tests,
475 Water Resour. Res., 47(3), 944-956, 2011.
476 Tong, M., Yuan, S., Ma, S., Jin, M., Liu, D., Cheng, D., and Wang, Y.: Production of
477 abundant hydroxyl radicals from oxygenation of subsurface sediments, Environ. Sci.
478 Technol., 50(1), 214-221, 2016.
479 Trudell, M. R., Gillham, R. W., and Cherry, J. A.: An in-situ study of the occurrence and rate
480 of denitrification in a shallow unconfined sand aquifer, J. Hydrol., 83(3), 251-268, 1986.
481 Wang, C. T., Yeh, H. D., and Tsai, C. S.: Transient drawdown solution for a constant
482 pumping test in finite two-zone confined aquifers. Hydrol. Earth Syst. Sci. Discuss.,
483 16(2), 441-449, 2012.
484 Wen, Z., Zhan, H. B., Huang, G. H., and Jin, M. G.: Constant-head test in a leaky aquifer
485 with a finite-thickness skin, J. Hydrol., 399(3-4), 326-334, 2011.
486 Yeh, H. D., Yang, S. Y., and Peng, H. Y.: A new closed-form solution for a radial two-layer
487 drawdown equation for groundwater under constant-flux pumping in a finite-radius well,
488 Adv. Water Resour., 26(7), 747-757, 2003.
489 Zimmermann, G., and Huenges, E.: Rock permeability and fluid pressure at the KTB.
490 implications from laboratory-and drill hole-measurements, Oil. Gas. Sci. Technol.,
491 54(6), 689-694, 1999.

Figure Captions:

Fig.1 The schematic diagram of the flow system.

Fig.2 Comparison between the numerical solutions of this study and the analytical solutions of Huang et al. (2010).

Fig.3 BTCs for different values of v_d at the well during the pumping phase.

Fig.4 The schematic diagram of the flow system for the pumping phase.

Fig.5 Concentration distributions in a 2D horizontal plane at t_{pump}=0 hr. a) $v_d = 1\times10^{-6}$ m/s,; b) $v_d = 1.5\times10^{-6}$m/s; c) $v_d = 2\times10^{-6}$ m/s; d) $v_d = 3\times10^{-6}$ m/s.

Fig.6 BTCs for different values of t_{res} at the well during the pumping phase.

Fig.7 Concentration distributions in a 2D horizontal plane at t_{pump}=0 hr. a) t_{res} = 6 hr; b) t_{res} = 126 hr; c) t_{res} = 24 hr; d) t_{res} = 36 hr.

Fig.8 BTCs at the well during the pumping phase with θ=0.1, 0.2, 0.3, 0.4, 0.5.

Fig.9 BTCs at the well during the pumping phase with α_L=0.01 m, 0.05 m, 0.1 m, 0.5 m.

Fig.10 BTCs for the case of a positive skin at the well during the pumping with r_s=0.6 m, and δ= 1, 0.5, 0.25 and 0.125.

Fig.11 2D horizontal plane distributions of concentration for a positive skin with r_s=0.6 m at t_{pump}=0 hr. a) δ= 1; b) δ= 0.5; c) δ= 0.25; d) δ= 0.125.

Fig.12 BTCs for the case of a negative skin at the well during the pumping with r_s=0.6 m, and δ= 1, 1.5, 2 and 3.

Fig.13 2D horizontal plane distributions of concentration for a negative skin with r_s=0.8 m at t_{pump}=0 hr. a) δ= 1; b) δ= 1.5; c) δ= 2; d) δ= 3.

Fig.14 BTCs for the case of a positive skin at the well during the pumping phase with r_s=0 m, 0.2 m, 0.4 m, 0.6 m.

515 Fig.15 Concentration distributions for a positive skin at 2D horizontal plane after 24 hr of

516 rest. a) r_s= 0 m; b) r_s= 0.2 m; c) r_s= 0.4 m; d) r_s= 0.6 m.

517 Fig.16 BTCs for the case of a negative skin at the well during the pumping with r_s=0 m,

518 0.2m, 0.4 m and 0.6 m.

519 Fig.17 Concentration distributions for a negative skin at 2D horizontal plane after 18 hr of

520 rest. a) r_s= 0 m; b) r_s= 0.2 m; c) r_s= 0.4 m; d) r_s= 0.6 m.

521

Hydrol. Earth Syst. Sci. Discuss., https://doi.org/10.5194/hess-2018-279
Manuscript under review for journal Hydrol. Earth Syst. Sci.
Discussion started: 18 July 2018

Hydrology and Earth System Sciences
Discussions
Open Access
EGU

522 Table 1. The parameter values used in this study

Parameter name	Symbols	Values
Aquifer thickness (m)	B	10
Radius of well screen (m)	r_w	0.1
Density of groundwater(kg/m^3)	ρ	1000
Effective porosity of aquifer	θ	0.3
Hydraulic conductivity of aquifer (m/d)	K	8
Constant heads of S_1(m)	H_1	15.22, 15.44, 15.69, 15.65, ,15.87, 16.08, 16.30
Constant head of S_2 (m)	H_2	15.0
Regional groundwater Darcy velocities (m/s)	v_d	5×10^{-7}, 1×10^{-6}, 1.5×10^{-6}, 2×10^{-6}, 2.5×10^{-6}, 3×10^{-6}
Longitudinal dispersivities of aquifer (m)	α_L	0.01, 0.05, 0.1, 0.5
Hydraulic conductivity of skin zone (m/d)	K_s	1, 2, 4, 12, 16, 24
Effective porosity of skin zone	θ_s	0.21,0.24,0.27,0.33,0.36,0.39
Injection or pumping rate (m^3/d)	Q	15, 30
Mass flux per unit area (kg/(m^2 • s))	N_0	0.02765, 0.5529
Injection time (hr)	t_{inj}	6
Rest time (hr)	t_{res}	24

Hydrol. Earth Syst. Sci. Discuss., https://doi.org/10.5194/hess-2018-279
Manuscript under review for journal Hydrol. Earth Syst. Sci.
Discussion started: 18 July 2018

Pumping time (hr)	t_{pump}	48

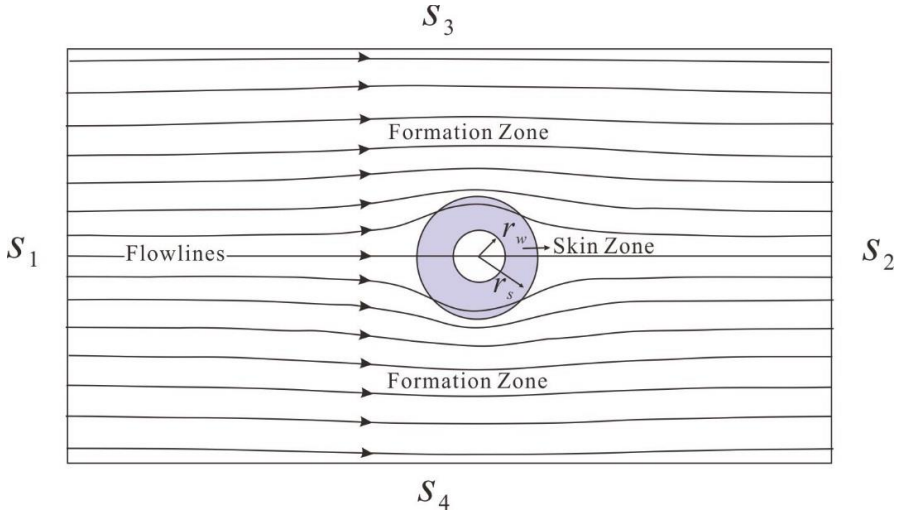

Fig.1

Hydrol. Earth Syst. Sci. Discuss., https://doi.org/10.5194/hess-2018-279
Manuscript under review for journal Hydrol. Earth Syst. Sci.
Discussion started: 18 July 2018

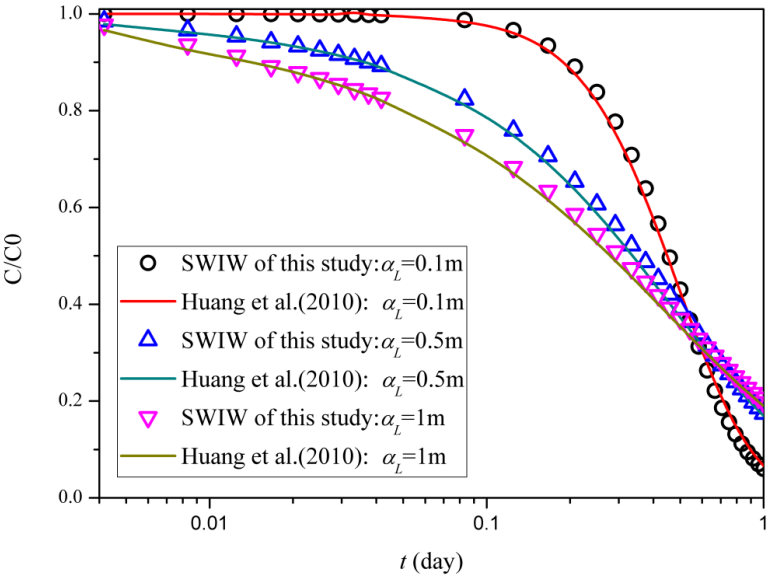

529

530

531

532

533

534 **Fig.2**

Hydrol. Earth Syst. Sci. Discuss., https://doi.org/10.5194/hess-2018-279
Manuscript under review for journal Hydrol. Earth Syst. Sci.
Discussion started: 18 July 2018

Hydrology and Earth System Sciences
Discussions

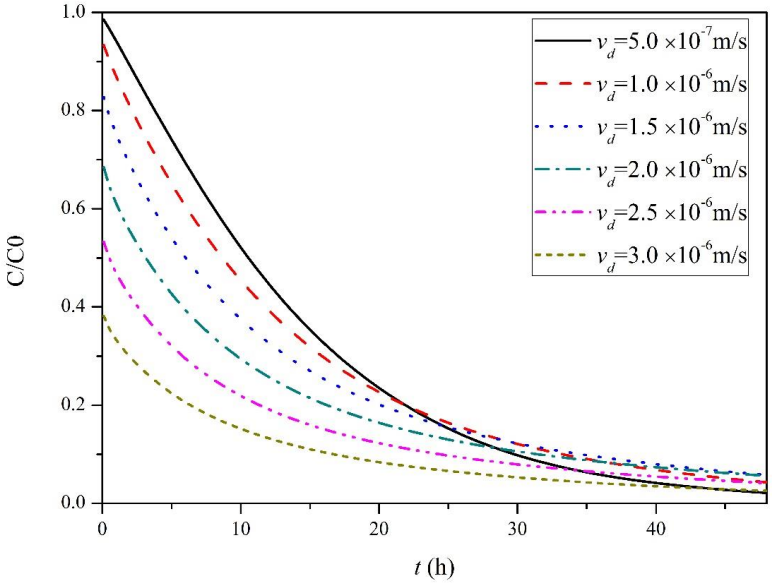

535

536

537

538

539 **Fig.3**

Hydrol. Earth Syst. Sci. Discuss., https://doi.org/10.5194/hess-2018-279
Manuscript under review for journal Hydrol. Earth Syst. Sci.
Discussion started: 18 July 2018

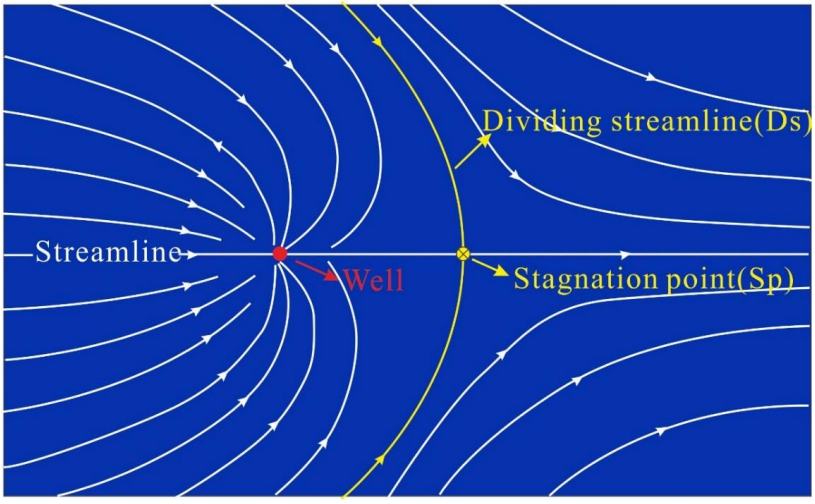

Fig.4

Hydrol. Earth Syst. Sci. Discuss., https://doi.org/10.5194/hess-2018-279
Manuscript under review for journal Hydrol. Earth Syst. Sci.
Discussion started: 18 July 2018

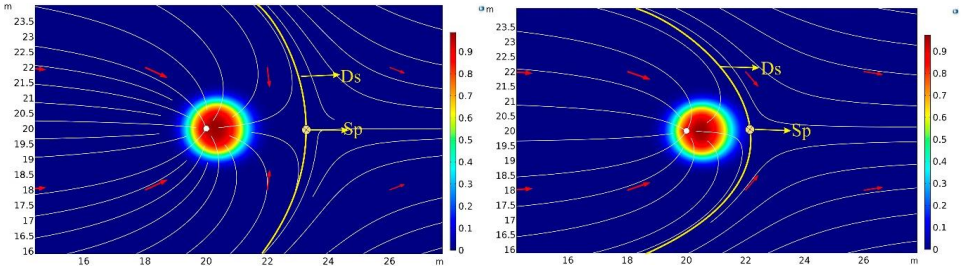

a. v_d =1×10^{-6}m/s b. v_d =1.5×10^{-6}m/s

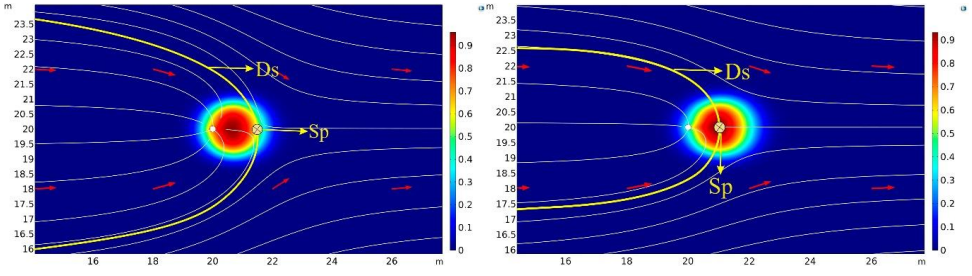

c. v_d =2×10^{-6}m/s d. v_d =3×10^{-6}m/s

Fig.5

Hydrol. Earth Syst. Sci. Discuss., https://doi.org/10.5194/hess-2018-279
Manuscript under review for journal Hydrol. Earth Syst. Sci.
Discussion started: 18 July 2018

Hydrology and Earth System Sciences
Discussions

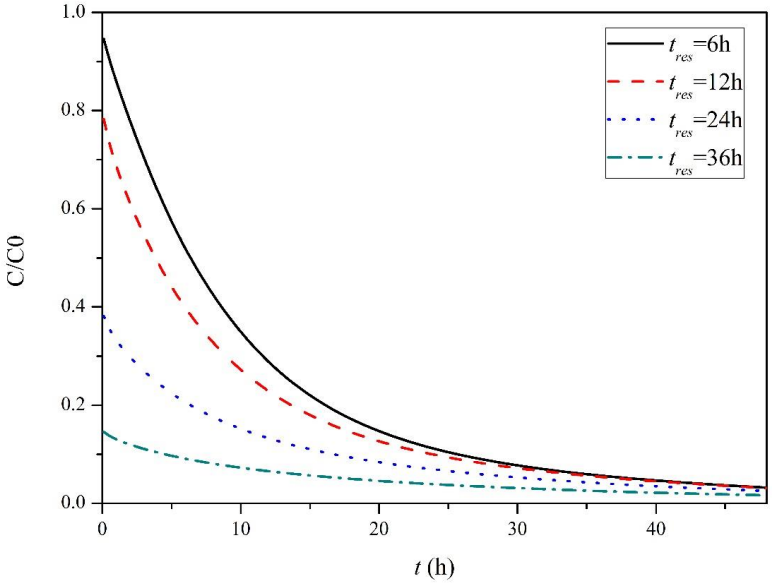

556

557

558

559 Fig.6

Hydrol. Earth Syst. Sci. Discuss., https://doi.org/10.5194/hess-2018-279
Manuscript under review for journal Hydrol. Earth Syst. Sci.
Discussion started: 18 July 2018

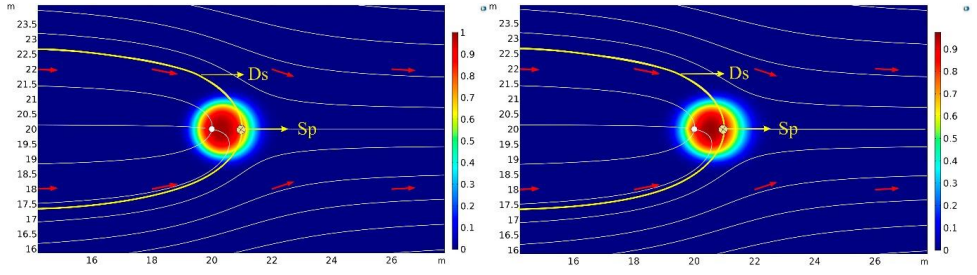

a. t_{res}= 6h b. t_{res}= 12h

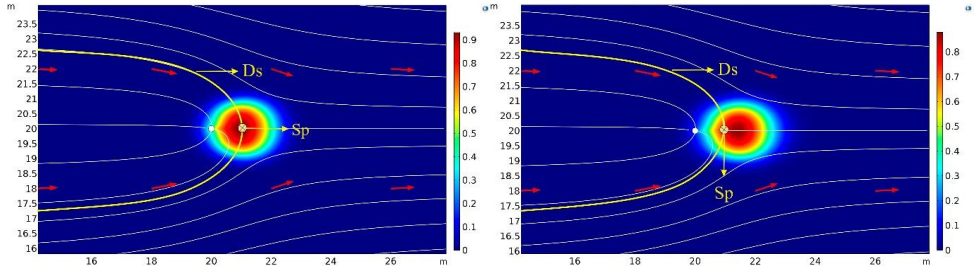

c. t_{res}= 24h d. t_{res}= 36h

Fig.7

Hydrol. Earth Syst. Sci. Discuss., https://doi.org/10.5194/hess-2018-279
Manuscript under review for journal Hydrol. Earth Syst. Sci.
Discussion started: 18 July 2018

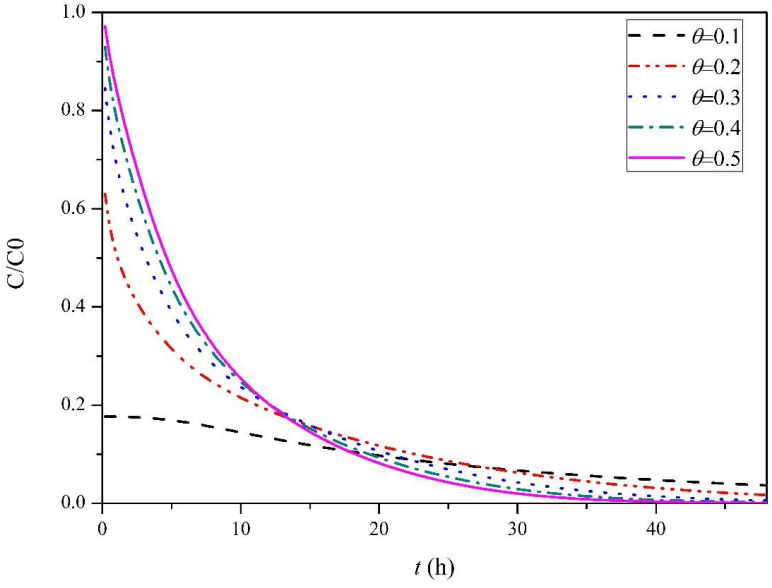

569

570

571

572 Fig.8

Hydrol. Earth Syst. Sci. Discuss., https://doi.org/10.5194/hess-2018-279
Manuscript under review for journal Hydrol. Earth Syst. Sci.
Discussion started: 18 July 2018

573

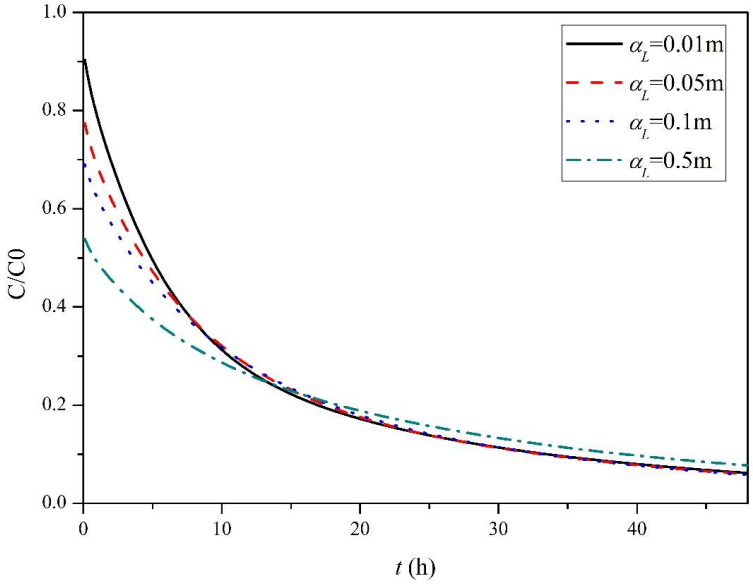

574

575

576

577 **Fig. 9**

Hydrol. Earth Syst. Sci. Discuss., https://doi.org/10.5194/hess-2018-279
Manuscript under review for journal Hydrol. Earth Syst. Sci.
Discussion started: 18 July 2018

Hydrology and Earth System Sciences
Discussions

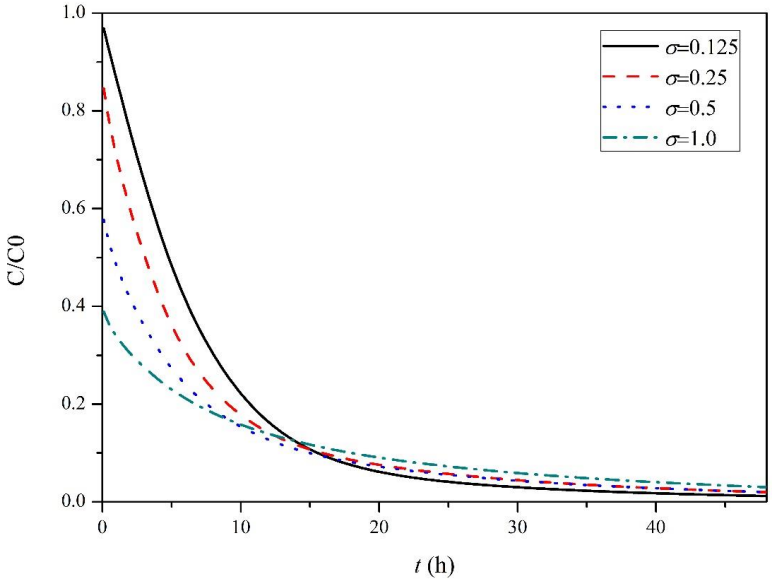

578

579

580

581

582

583 **Fig.10**

Hydrol. Earth Syst. Sci. Discuss., https://doi.org/10.5194/hess-2018-279
Manuscript under review for journal Hydrol. Earth Syst. Sci.
Discussion started: 18 July 2018

584 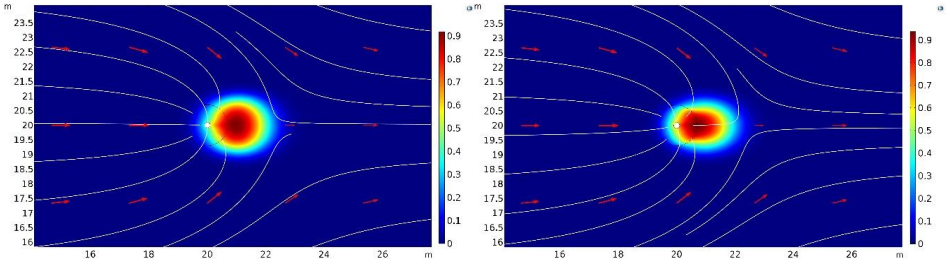

585 a. δ=1 b. δ=0.5

586 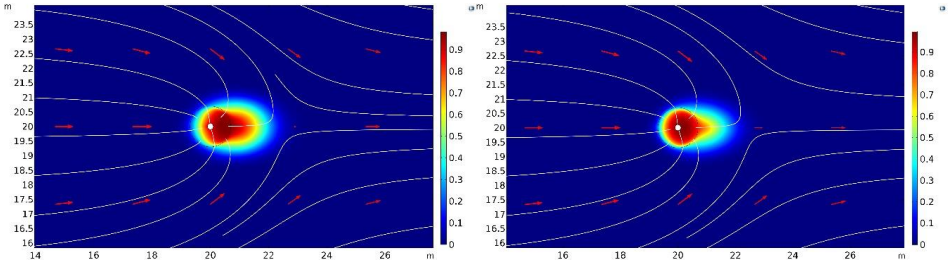

587 c. δ=0.25 d. δ=0.125

588

589 **Fig.11**

Hydrol. Earth Syst. Sci. Discuss., https://doi.org/10.5194/hess-2018-279
Manuscript under review for journal Hydrol. Earth Syst. Sci.
Discussion started: 18 July 2018

Hydrology and Earth System Sciences
Discussions

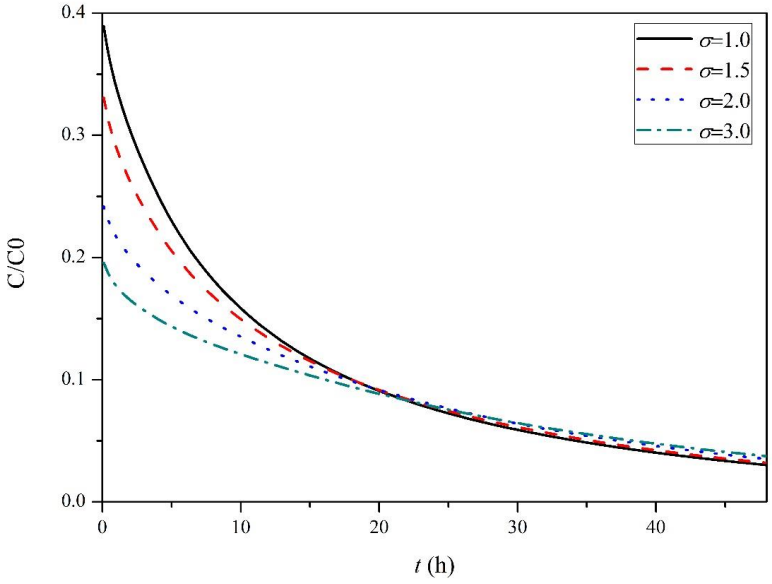

590

591

592

593

594 **Fig.12**

Hydrol. Earth Syst. Sci. Discuss., https://doi.org/10.5194/hess-2018-279
Manuscript under review for journal Hydrol. Earth Syst. Sci.
Discussion started: 18 July 2018

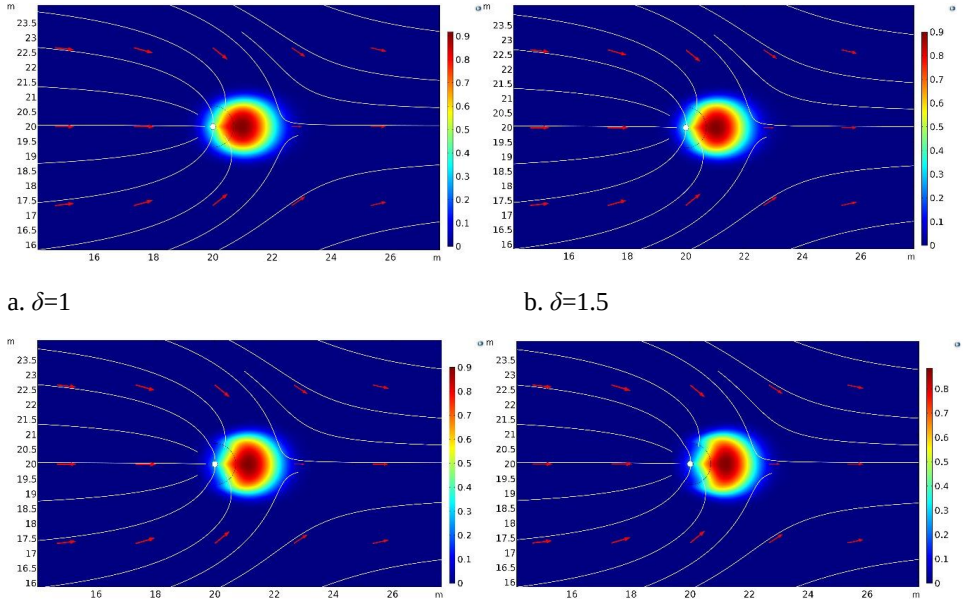

a. δ=1 b. δ=1.5

c. δ=2 d. δ=3

Fig.13

Hydrol. Earth Syst. Sci. Discuss., https://doi.org/10.5194/hess-2018-279
Manuscript under review for journal Hydrol. Earth Syst. Sci.
Discussion started: 18 July 2018

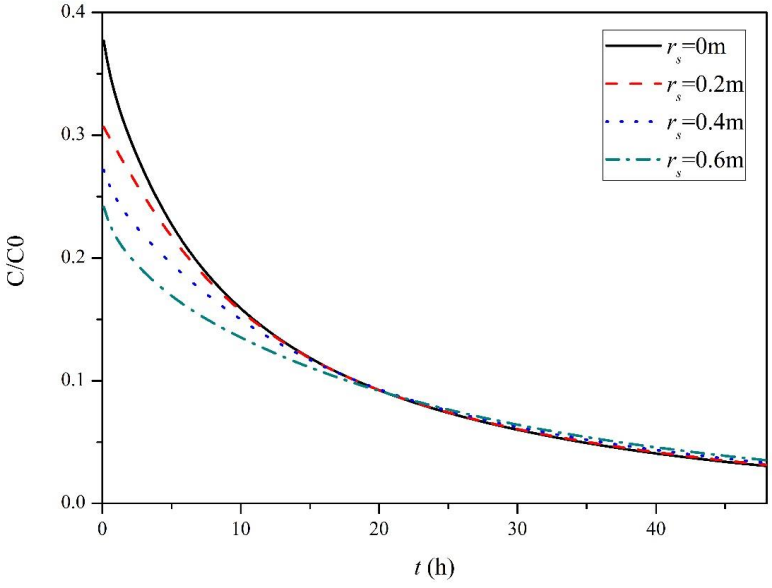

602

603

604

605

606 **Fig.14**

Hydrol. Earth Syst. Sci. Discuss., https://doi.org/10.5194/hess-2018-279
Manuscript under review for journal Hydrol. Earth Syst. Sci.
Discussion started: 18 July 2018

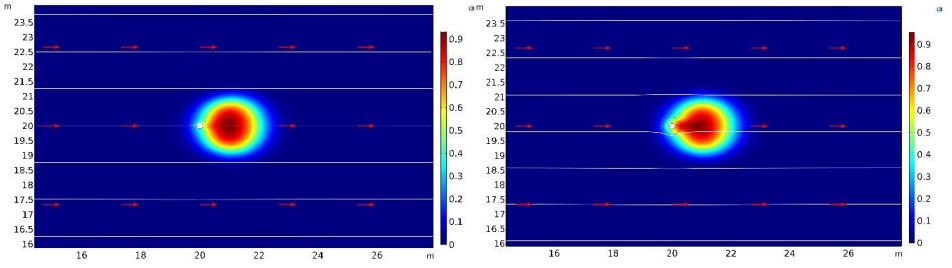

a. r_s =0 m b. r_s =0.2 m

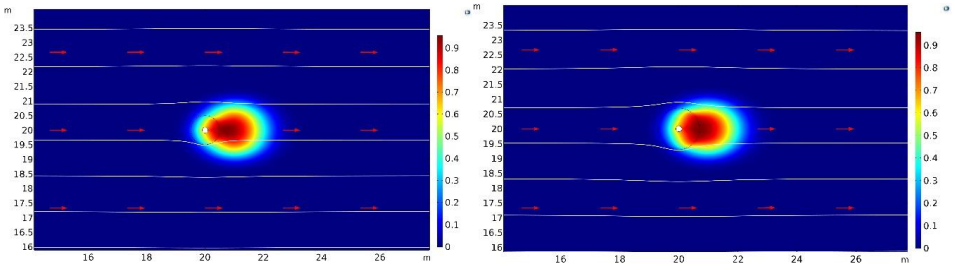

c. r_s =0.4 m d. r_s =0.6 m

Fig.15

Hydrol. Earth Syst. Sci. Discuss., https://doi.org/10.5194/hess-2018-279
Manuscript under review for journal Hydrol. Earth Syst. Sci.
Discussion started: 18 July 2018

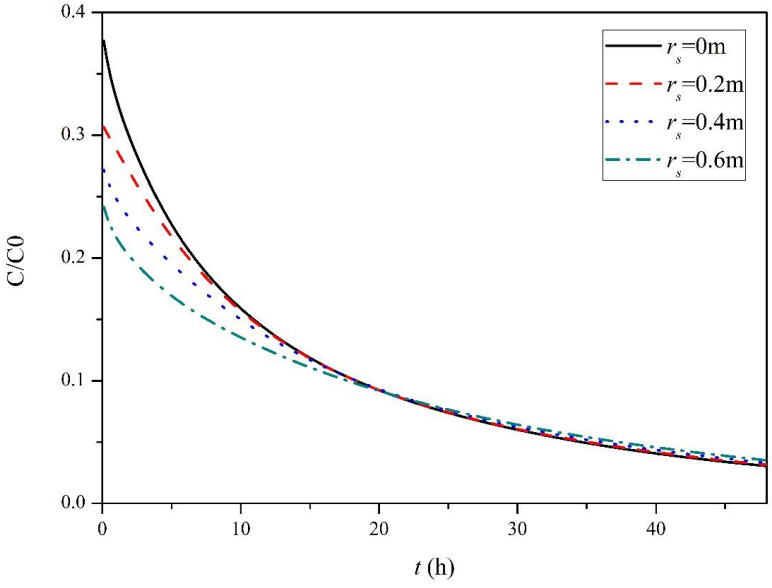

615

616

617

618

619 **Fig. 16**

Hydrol. Earth Syst. Sci. Discuss., https://doi.org/10.5194/hess-2018-279
Manuscript under review for journal Hydrol. Earth Syst. Sci.
Discussion started: 18 July 2018

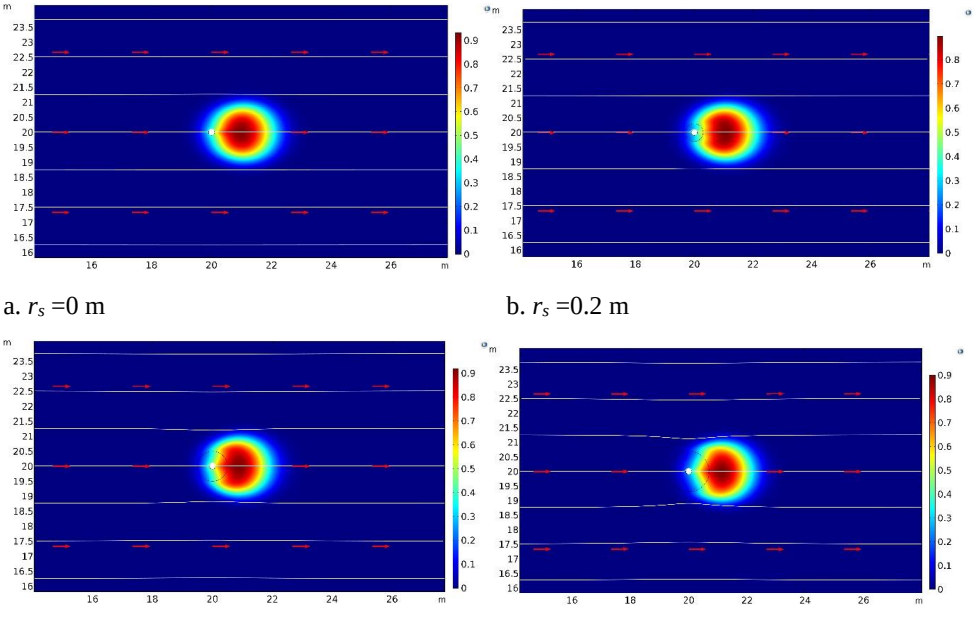

a. r_s =0 m b. r_s =0.2 m

c. r_s =0.4 m d. r_s =0.6 m

Fig. 17